International Journal of Nanomedicine

Dovepress
Taylor & Francis Group

Open Access Full Text Article

ORIGINAL RESEARCH

Exosomal BMPR2 Macromolecule Facilitates Alveolar Epithelial Cell Repair Through Functional Complex Formation with BMPR1B in Acute Lung Injury

Xiang Yun[1–3], Zhen Chen[4], Fei Li[1], Fuhai Shen[1], Lin Zhang[2,3,5], Juxiang Yuan[1]

[1]School of Public Health, North China University of Science and Technology, Tangshan, 063000, People's Republic of China; [2]Clinical Medical Research Center for Women and Children Diseases, Shandong Provincial Maternal and Child Health Care Hospital Affiliated to Qingdao University, Jinan, 250001, People's Republic of China; [3]Key Laboratory of Occupational Exposure and Fertility Preservation for Women of Shandong Health Commission, Shandong Provincial Maternal and Child Health Care Hospital Affiliated to Qingdao University, Jinan, 250001, People's Republic of China; [4]School of Public Health, Shandong Second Medical University, Weifang, 261053, People's Republic of China; [5]Henan Medical Key Laboratory for Research of Trauma and Orthopedics, The Third Affiliated Hospital of Xinxiang Medical University, Xinxiang, 453000, People's Republic of China

Correspondence: Juxiang Yuan, School of Public Health, North China University of Science and Technology, Tangshan, 063000, People's Republic of China, Email yuanjx@ncst.edu.cn; Lin Zhang, Clinical Medical Research Center for Women and Children Diseases, Shandong Provincial Maternal and Child Health Care Hospital Affiliated to Qingdao University, Jinan, 250001, People's Republic of China, Tel +86-531-68795920, Email zhanglin8901@sdu.edu.cn

Background: Acute lung injury (ALI) poses significant clinical challenges due to its irreversible alveolar damage and the limitation of available regenerative therapies. Emerging evidence suggests that macrophage-epithelial crosstalk plays a pivotal role in lung repair; however, the specific molecular mediators underlying this process remain largely undefined.

Methods: To address this gap, we isolated and characterized macrophage-derived exosomes (MD-Exos) using dynamic light scattering, transmission electron microscopy (TEM), and immunoblotting. Proteomic analysis and molecular docking were employed to reveal interactions between BMPR2 on exosomes and BMPR1B on epithelial cells. Single-cell RNA sequencing (scRNA-seq) was utilized to map alveolar cell dynamics. Biochemical assays and confocal colocalization were performed to validate SMAD1 signaling activation. The biodistribution of exosomes was tracked via near-infrared imaging, and AT2-to-AT1 transdifferentiation was assessed through multiplex immunofluorescence and pseudotime trajectory analysis.

Results: Proteomic profiling of MD-Exos identified BMPR2 as the predominant component. Molecular docking studies confirmed a strong binding affinity between exosomal BMPR2 and epithelial BMPR1B. Single-cell RNA sequencing and biochemical analyses revealed significant alterations in alveolar macrophage (34% vs 27%) and epithelial cell populations during injury, accompanied by enhanced cellular communication. The characterized macrophage-derived exosomes (163.6 ± 70.2 nm) demonstrated efficient pulmonary targeting, with peak accumulation occurring at 4 hours post-administration. Mechanistically, the formation of the BMPR2-BMPR1B complex activated SMAD1-dependent signaling pathways, as evidenced by strong BMPR1B-SMAD1 colocalization (correlation coefficient 0.94 ± 0.02) and enhanced ID1 expression.

Conclusion: The BMPR2-BMPR1B interaction was demonstrated to accelerate type II to type I alveolar epithelial cell transdifferentiation, thereby facilitating tissue repair in ALI. Comprehensive toxicological assessment confirmed the safety profile of exosome administration across major organ systems. These findings establish exosomal BMPR2 as a crucial mediator of pulmonary repair through specific molecular recognition and signaling activation, providing new therapeutic strategies for treating acute lung injury.

Keywords: exosomal BMPR2, BMPR1B, alveolar epithelial cells, cellular repair, protein-protein interaction

Introduction

Acute lung injury (ALI) represents a complex pathophysiological syndrome characterized by rapid-onset respiratory dysfunction, diffuse alveolar damage, and severe gas exchange impairment.[1,2] Despite advances in critical care medicine,

Received: 13 March 2025
Accepted: 31 May 2025
Published: 7 June 2025

Graphical Abstract

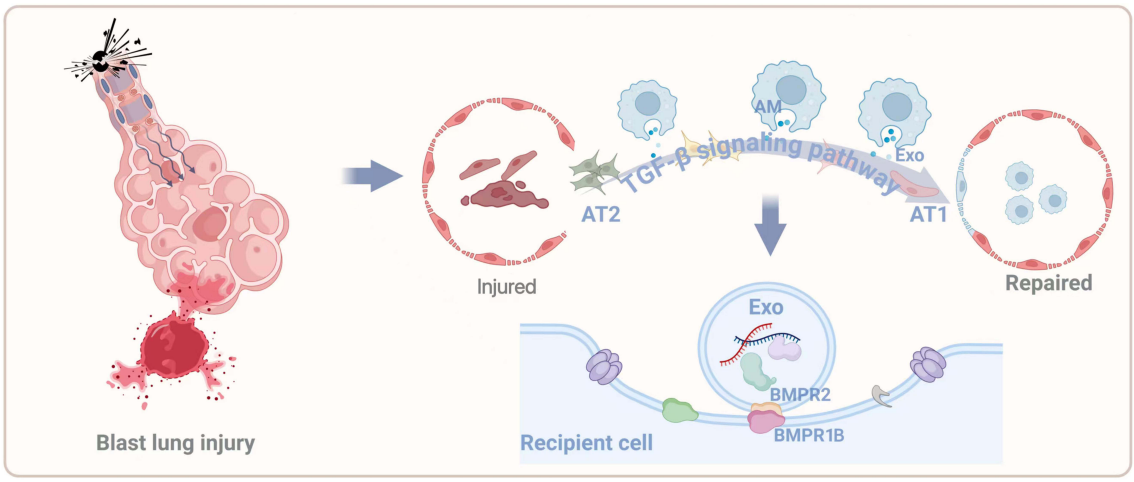

ALI and its severe form, acute respiratory distress syndrome (ARDS), continue to exhibit mortality rates ranging from 35% to 46%.[3] The pathogenesis involves intricate interactions between mechanical trauma, inflammatory cascades, and cellular dysfunction, leading to disruption of the alveolar-capillary barrier, pulmonary edema, and compromised gas exchange.[4,5]

Recent advances in cellular biology have highlighted the crucial role of extracellular vesicles, particularly exosomes (30–150 nm diameter), in mediating intercellular communication and tissue repair processes.[6,7] These nano-sized lipid bilayer vesicles, secreted by virtually all cell types, function as sophisticated carriers of bioactive molecules, including membrane-bound proteins that can directly interact with target cell receptors.[8,9] Among these proteins, biological macromolecules such as bone morphogenetic protein receptors (BMPRs) have emerged as particularly important mediators of cellular communication and tissue repair.[10] Emerging evidence indicates that bone morphogenetic protein (BMP) and its receptors, particularly the BMPR2 receptor, exert anti-fibrotic effects by antagonizing TGF-β-mediated signaling pathways. Upregulating BMPR2 through targeted signaling transduction can effectively suppress TGF-β-induced pro-fibrotic responses in pulmonary fibroblasts.[11,12]

The BMPR family, comprising type I (BMPR1A and BMPR1B) and type II (BMPR2) receptors, plays crucial roles in development, homeostasis, and tissue repair. BMPR2, a serine/threonine kinase receptor, has garnered significant attention due to its involvement in various physiological and pathological processes.[13] Recent studies have demonstrated that BMPR2 mutations are associated with pulmonary arterial hypertension and impaired tissue repair, highlighting its importance in maintaining pulmonary homeostasis. The presence of BMPR2 on exosomal surfaces represents a novel mechanism for intercellular communication, particularly in the context of tissue repair.[14,15]

Within the complex cellular network of the lung, alveolar macrophages emerge as critical orchestrators of both inflammatory responses and repair processes.[16] These cells exhibit remarkable plasticity in their response to injury, particularly through their secretion of regulatory factors and exosomes. Of particular interest is the bidirectional communication between macrophages and alveolar epithelial type II cells (AT2), which forms a crucial axis in lung homeostasis and repair. Recent evidence suggests that macrophage-derived exosomes may serve as key mediators in this cellular dialogue, particularly through the interaction of exosomal BMPR2 with cellular receptors.[17,18] However, the molecular mechanisms underlying exosome-mediated tissue repair, particularly the role of surface proteins in target cell recognition and signaling activation, remain incompletely understood. While previous studies have demonstrated the therapeutic potential of exosomes in various disease models, the specific contribution of exosomal BMPR2 and its

interaction with target cell receptors has not been fully elucidated. Understanding these molecular interactions is crucial for developing targeted therapeutic strategies.

Building upon these observations and considering the established role of BMPR signaling in tissue repair, we hypothesized that macrophage-derived exosomal BMPR2 facilitates targeted intercellular communication through specific interaction with BMPR1B on injured alveolar epithelial cells. To test this hypothesis, we employed a systematic approach beginning with proteomic analysis of macrophage-derived exosomes, followed by detailed characterization of BMPR2-BMPR1B interactions and their downstream effects on cellular repair processes.

This study aims to elucidate the molecular mechanisms through which exosomal BMPR2 mediates communication between immune cells and damaged alveolar epithelium, potentially offering new therapeutic strategies for acute lung injury. Understanding these complex protein-protein interactions and their downstream effects is crucial for developing targeted interventions that can effectively promote lung repair and regeneration. Our findings provide novel insights into the role of exosomal membrane proteins in cellular communication and tissue repair, with broad implications for therapeutic development in various pathological conditions.

Methods and Materials

Animals and in vivo ALI Model Establishment

The experimental protocol was approved by the Institutional Ethics Committee of Shandong Maternal and Child Health Hospital (Approval No. 2022–006), and all animal procedures strictly followed the National Research Council's Guide for the Care and Use of Laboratory Animals (8th ed., 2011). The research involved 40 adult male C57BL/6 mice (age: 8–9 weeks; weight: 18–20 g) obtained from Pengyue Experimental Animals in Jinan (license: SCXK (LU) 20220006). Prior to experimentation, the animals underwent a one-week acclimation period in the specific pathogen-free facility at the Third Affiliated Hospital of Xinxiang Medical College. The experimental setup employed a patented shock tube apparatus (CN112630266A; Northern Petrochemical Equipment Factory, Liaoning) designed to simulate coal mine gas explosions. The apparatus integrates explosion chamber components with systems for ignition, gas distribution, and comprehensive data collection including pressure and temperature measurements. Based on previous investigations by our research group,[19] we established optimal explosion parameters. The protocol involved preparing a 30-liter methane mixture at 10% concentration via partial pressure methodology. Shock wave generation was achieved through high-voltage electrode ignition, with wall-mounted sensors capturing key explosion parameters including peak overpressure, phase duration, and maximum temperature. To maintain experimental consistency, we implemented standardized animal positioning protocols. Following system integrity verification, anesthetized mice were secured supinely in specialized cages, with thoracic regions facing the explosion source. The subjects were positioned perpendicular to the shock tube axis at a fixed distance of 1.6 meters from the sealing membrane. Groups of five animals underwent sequential shock wave exposure. Post-exposure monitoring occurred in pathogen-free conditions over periods of 1, 3, 7 days, with continuous vital sign assessment. At each predetermined endpoint, five animals per group were humanely euthanized for pulmonary tissue evaluation, specifically examining hemorrhage, edema, and inflammatory cell infiltration.

Isolation and Characterization of J774A.1 Macrophage-Derived Exosomes

To elucidate the role of macrophage-derived exosomes in intercellular repair mechanisms, we implemented a systematic protocol for exosome isolation from J774A.1 (CL-3070, ProCell, Wuhan, China) mononuclear macrophages using differential ultracentrifugation. The isolation process began with cultivating J774A.1 cells to greater than 95% confluence to ensure optimal exosome yield. To eliminate potential contamination from serum-derived exosomes, we transitioned the cultures to serum-free medium and maintained them for an additional 12-hour period prior to supernatant collection.

The isolation protocol consisted of sequential centrifugation steps designed to progressively separate exosomes from other cellular components. Initially, the collected supernatant underwent a series of differential centrifugation steps: 500 g for 10 minutes, followed by 2,000 g for 15 minutes, and 10,000 g for 30 minutes. The resulting supernatant was then filtered through a 0.22 μm membrane to remove remaining larger particles. The final isolation step involved ultracentrifugation at 120,000 g for 70 minutes, after which the isolated exosome pellet was washed and resuspended in

phosphate-buffered saline (PBS). The purified exosome preparation was stored in 1.5 mL EP tubes at −80°C for subsequent analyses. Comprehensive characterization of the isolated exosomes involved multiple analytical approaches. Morphological examination was conducted using transmission electron microscopy. In order to ensure sample integrity for downstream applications, quantitative assessment of particle size distribution and concentration was performed through a combination of nanoparticle tracking analysis and dynamic light scattering technology.

Hematoxylin and Eosin Staining (H&E) Test

Histopathological examination of mouse lung tissue was conducted using standardized hematoxylin and eosin (H&E) staining protocols to evaluate structural changes following exposure to explosion conditions. The preparation process began with tissue fixation in 4% formaldehyde solution for 24 hours to preserve cellular architecture. Following fixation, the tissue specimens underwent sequential dehydration steps before paraffin embedding. The embedded tissue blocks were sectioned into thin slices and carefully mounted on microscope slides for staining. The dual-staining procedure commenced with the application of hematoxylin, which selectively binds to acidic cellular components, particularly nuclear material, producing characteristic blue-violet chromatin staining. Subsequently, the sections were counterstained with eosin to visualize basic cellular elements, including cytoplasmic proteins and extracellular matrix components, which acquired a distinctive pink coloration. Following the staining sequence, the tissue sections underwent final dehydration and clearing with xylene before permanent mounting with coverslips. Microscopic evaluation and digital image acquisition were performed using the VS200 whole-slide scanning system (VS200, Olympus, Japan), enabling comprehensive analysis of explosion-induced pathological alterations in the pulmonary tissue architecture.

Immunofluorescence Assay

Lung tissue specimens underwent fixation in 4% paraformaldehyde for 10 minutes at room temperature, followed by three 5-minute washes with 1× PBS. Tissue permeabilization was performed using 0.3% Triton X-100 for 15 minutes at room temperature, with subsequent triple PBS washing. Non-specific binding was blocked using 10% goat serum for 60 minutes at room temperature. Primary antibody application (50 μL per slide) proceeded with overnight incubation at 4°C in a light-protected environment. Following primary antibody removal and washing, fluorescent-conjugated secondary antibodies were applied and incubated for 120 minutes at room temperature under dark conditions. Nuclear visualization employed DAPI staining (50 μL) for 15 minutes at room temperature. The specimens were mounted using anti-fluorescence quenching medium and analyzed using the ImageXpress® Micro-Confocal System.

Immunohistochemistry Assay

Following standard H&E processing and antigen retrieval, tissue sections were treated with 50 μL of 3% hydrogen peroxide for 25 minutes at room temperature to quench endogenous peroxidase activity. After three 5-minute PBS washes, sections underwent blocking with 50 μL of 5% fetal bovine serum albumin for 30 minutes. Secondary antibody application proceeded for 60 minutes at room temperature, followed by three PBS washes. Visualization was achieved using 100 μL DAB chromogen (10-minute incubation), with subsequent hematoxylin counterstaining (100 μL, 3 minutes). The sections underwent differentiation for 10 seconds and sequential dehydration through 75%, 85%, and absolute ethanol, followed by xylene clearing (5 minutes per step). Permanent mounting used neutral resin, with imaging performed via the VS200 whole-slide scanning system.

Western Blot Assay

Tissue and cellular proteins were extracted using RIPA lysis buffer, with concentration determination by BCA assay. Samples were prepared in 4:1 sample-to-buffer ratio and denatured at 100°C for 10 minutes. Protein separation employed concentration-appropriate SDS-PAGE gels, with initial electrophoresis at 80 V followed by 120 V completion. Methanol-activated PVDF membranes were used for protein transfer at 230 mA (40–70 minutes, depending on molecular weight). Following triple 7-minute TBST washes, membranes were blocked with 5% skim milk for 60 minutes at room temperature. Primary antibody incubation proceeded overnight at 4°C, followed by three TBST washes and 60-minute

secondary antibody incubation. Protein visualization employed chemiluminescent detection via the ChemiDoc MP system, with quantitative analysis using ImageJ software.

In vivo Exosome Tracking

J774A.1-derived exosomes were fluorescently labeled using DiO dye through 4-hour room temperature incubation. Labeled exosomes (10 μL) were administered via intratracheal instillation to depilated mice. The IVIS spectral CT system was employed for fluorescence imaging at 0, 1, 2, 4, 8, 16, and 24 h post-administration, using three animals per time point. Pulmonary fluorescence intensity was quantified using in vivo Image V4.4 software, enabling temporal tracking of exosome biodistribution.

Cellular Thermal Shift Assay

Lung tissues from ALI and ALI+Exo (ALI treated with exosomes) group mice were collected. Equal weights of lung tissue homogenates were prepared and aliquoted into multiple 2 mL EP tubes. These aliquots were subjected to a metal bath for thermal denaturation at distinct temperatures (37°C, 45°C, 48°C, 50°C, and 53°C) for 5 minutes each. Following heating, samples were rapidly cooled on ice to terminate protein denaturation. Tissue proteins were subsequently extracted using RIPA lysis buffer. The lysates were centrifuged at 20,000 g for 20 min at 4°C to collect undegraded protein supernatants. Protein concentrations were measured using a BCA assay kit. Loading buffer was added to the samples, which were then denatured at 100°C for 10 min. Equal amounts of protein from each sample were loaded for SDS-PAGE electrophoresis, and residual expression of target proteins was analyzed via Western Blot. Thermal stability curves (temperature vs protein residual level) were plotted to evaluate protein stability.

Statistical Analysis

All experimental data generated in this study underwent comprehensive processing and analysis using multiple statistical platforms. Initial data consolidation was performed in Microsoft Excel 2019, followed by rigorous quality control, statistical analysis, and visualization using R v4.4.1 for Windows. Additional data analysis was conducted using GraphPad Prism 9.4 for Windows. Continuous data were subjected to normality testing to determine appropriate statistical approaches. For comparisons between two groups, Student's *t*-test was employed, while multiple group comparisons utilized one-way analysis of variance (ANOVA) followed by Student-Newman-Keuls post hoc tests. Statistical significance was established at $P < 0.05$ unless otherwise specified.

Results

Blast Induces Progressive Pulmonary Inflammation and Acute Lung Injury in vivo

To elucidate the pathophysiological mechanisms of BLI, we established a controlled blast exposure model using C57BL/6 mice. Animals were subjected to blast waves characterized by a maximum overpressure of 0.467 ± 0.04 MPa with a peak pressure time of 245.8 ± 0.12 ms, parameters optimized based on our previous investigations. Longitudinal analyses were performed at 1, 3, and 7 days post-exposure to assess the progression of pulmonary pathology (Figure 1A). After exposure to blast wave, 5 mice died and the survival rate was 75% (15/20). Physiological monitoring revealed divergent weight trajectories between experimental groups, with control mice maintaining normal weight gain patterns, while blast-exposed animals exhibited significant progressive weight loss throughout the observation period (Figure 1B). Histopathological evaluation using H&E staining demonstrated that control mice maintained physiological pulmonary architecture, characterized by thin-walled alveoli lined with continuous single-layer epithelium, patent alveolar spaces, and absence of inflammatory infiltrates. In contrast, blast-exposed mice developed severe architectural disruption, manifested by marked alveolar wall thickening, extensive inflammatory cell infiltration, and progressive development of fibrotic changes over the experimental time course (Figure 1C).

The phenotypic transition of alveolar epithelial type II (AT2) cells to type I (AT1) cells represents a critical regulatory mechanism in pulmonary repair following acute injury. To characterize this process, we analyzed the temporal expression patterns of canonical cell type-specific markers: AGER and AQP1 for AT1 cells, and SFTPD and SFTPA1 for AT2 cells.

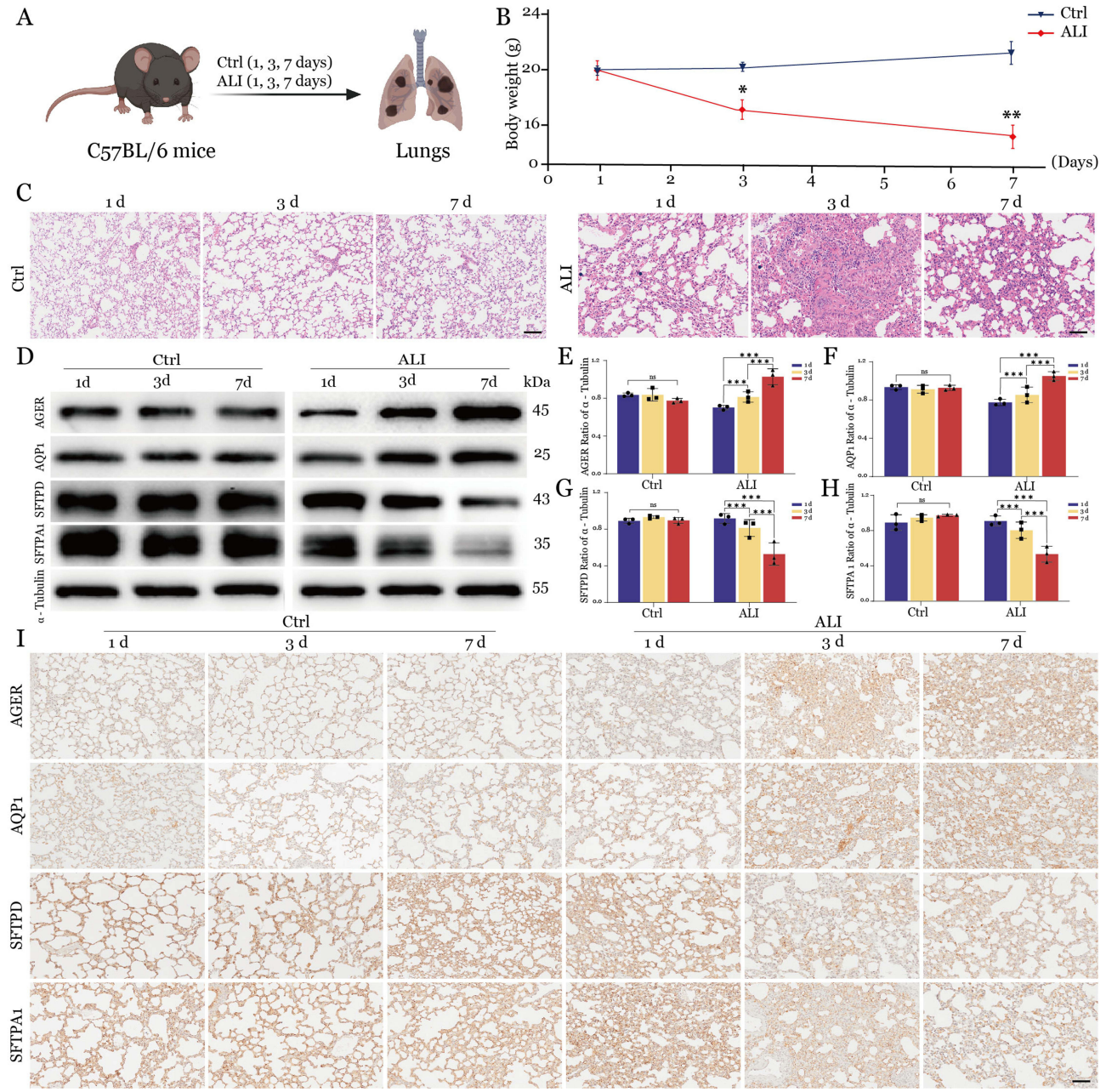

Figure 1 Establishment of acute lung injury mouse model and assessment of type I/II alveolar epithelial cell damage. **(A)** Schematic representation of the shock tube apparatus used to establish the act lung injury (ALI) mouse model. **(B)** Temporal changes in body weight of BLI model mice over 7 days post-blast. Statistical significance compared to time-matched controls is indicated (*P < 0.05, **P < 0.01). **(C)** Representative hematoxylin and eosin (H&E) staining of lung tissue sections from BLI mice demonstrating pathological changes. **(D)** Western blot showing the expression of type I (AQP1 and AGER) and type II (SFTPA1 and SFTPD) alveolar epithelial cell marker proteins. **(E–H)** Quantitative densitometric analysis of AQP1, AGER, SFTPA1, and SFTPD protein expression (ns, no significant; ***P < 0.001). **(I)** Immunohistochemistry analysis of type I/II alveolar epithelial cell markers in BLI mouse lung tissue. Nuclei are visualized in blue, with positive protein expression indicated by brown-yellow staining. Scale bar = 100 nm.

Quantitative Western blot analyses revealed that blast-exposed mice demonstrated time-dependent alterations in these cellular markers compared to controls, with progressive upregulation of AGER and AQP1 expression, concurrent with significant downregulation of SFTPD and SFTPA1 levels across days 1, 3, and 7 post-exposures (Figure 1D-H). These molecular alterations were further validated through immunohistochemical and immunofluorescence analyses, which confirmed the temporal dynamics of cell type-specific marker expression in pulmonary tissue sections (Figure 1I, Figure S1). Collectively, these findings demonstrate that blast exposure induces severe acute lung injury characterized by

progressive weight loss, sustained inflammatory cell infiltration, and significant dysregulation of key proteins essential for pulmonary homeostasis. The persistence and progression of these pathological alterations through day 7 post-exposure provide a robust experimental framework for subsequent mechanistic investigations. Based on the temporal profile of these changes, we identified day 7 post-blast exposure as the optimal time point for detailed molecular and cellular analyses in subsequent experiments.

Single-Cell RNA Sequencing Analysis Reveals Enhanced BMPR1B Expression in Injured Alveolar Epithelial Cells

To characterize the cellular dynamics and receptor expression patterns in injured lung tissue, we performed single-cell RNA sequencing reanalysis based on our previous data (Figure 2A).[19] Unsupervised clustering identified nine distinct cell populations, with alveolar epithelial cells and macrophages showing significant alterations in their relative proportions (AM: 27% vs 34%; AT1: 13% vs 17%; AT2: 4% vs 12%) (Figure 2B-D). Notably, injured alveolar epithelial cells demonstrated markedly increased BMPR1B expression compared to controls, with a 1.99-fold increase in transcript levels (Figure 2E). This upregulation was particularly pronounced in type II alveolar epithelial cells, which showed concurrent changes in canonical cell-type markers (Figure 2F-G). Integration analysis using STRING protein-protein interaction database positioned the BMPR1B-centered signaling pathways as a central regulatory hub, with BMPR1B emerging as a key node in the cellular response to injury (Figure 2H).

Proteomic Characterization of Macrophage-Derived Exosomes Reveals BMPR2 as a Key Surface Protein

As resident immune cells exhibiting functional diversity and high plasticity, alveolar macrophages play crucial roles in acute lung injury repair. Transmission electron microscopy analysis of isolated exosomes revealed characteristic cup-shaped structures with round or oval morphology, appearing both as individual vesicles and in clusters (Figure 3A). Western blot analysis confirmed the expression of canonical exosome markers CD9, CD63, CD81, TSG101 and BMPR2 (Figure 3B). Nanoparticle tracking analysis and dynamic light scattering characterized the isolated vesicles with an average diameter of 163.6 ± 70.2 nm and concentration of 1.89×10^{11}/mL (Figure 3C).

To identify potential therapeutic mediators in macrophage-derived exosomes, we performed comprehensive proteomic analysis using high-resolution mass spectrometry. Exosomes isolated from J774A.1 macrophages were subjected to sequential extraction procedures to separate proteins. Mass spectrometric analysis identified a total of 3,603 unique proteins (Figure 3D), with 1,247 classified as membrane-associated based on GO cellular component analysis (Figure 3E). Among these, BMPR2 emerged as one of the most abundant membrane proteins, placing it in the top 55% of all identified membrane proteins. These findings collectively establish BMPR2 as a major functional component of macrophage-derived exosomes.

The Strong Affinity Functional Complex of Extracellular Vesicle BMPR2 and Cellular BMPR1B Can Alleviate ALI Inflammatory Response

To investigate the potential interaction between exosomal BMPR2 and cellular BMPR1B, we first performed in silico molecular docking studies. Crystal structures of BMPR2 (PDB: 3G2F) and BMPR1B (PDB: 3MDY) were subjected to extensive docking simulations using the AutoDock Vina platform. Initial rigid body docking generated 200 possible conformations, which were filtered based on interaction energy and biological plausibility. Subsequently, we utilized the HDOCK molecular docking technology (http://hdock.phys.hust.edu.cn/) to conduct a thorough simulation analysis of the interaction between BMPR2 and BMPR1B proteins (Figure 4A). The analysis revealed that the first model had a Docking Score of −246.20, indicating a strong affinity between the two proteins. The confidence score of 0.8726 further corroborates the high reliability of our predictions regarding their interaction. Additionally, the Ligand RMSD of 91.98 Å suggests minimal conformational changes during the docking process, which is beneficial for establishing a stable protein-protein interaction. These findings were further supported by chemical cross-linking studies followed by mass spectrometric analysis, which identified multiple cross-links between regions predicted to be in close proximity in

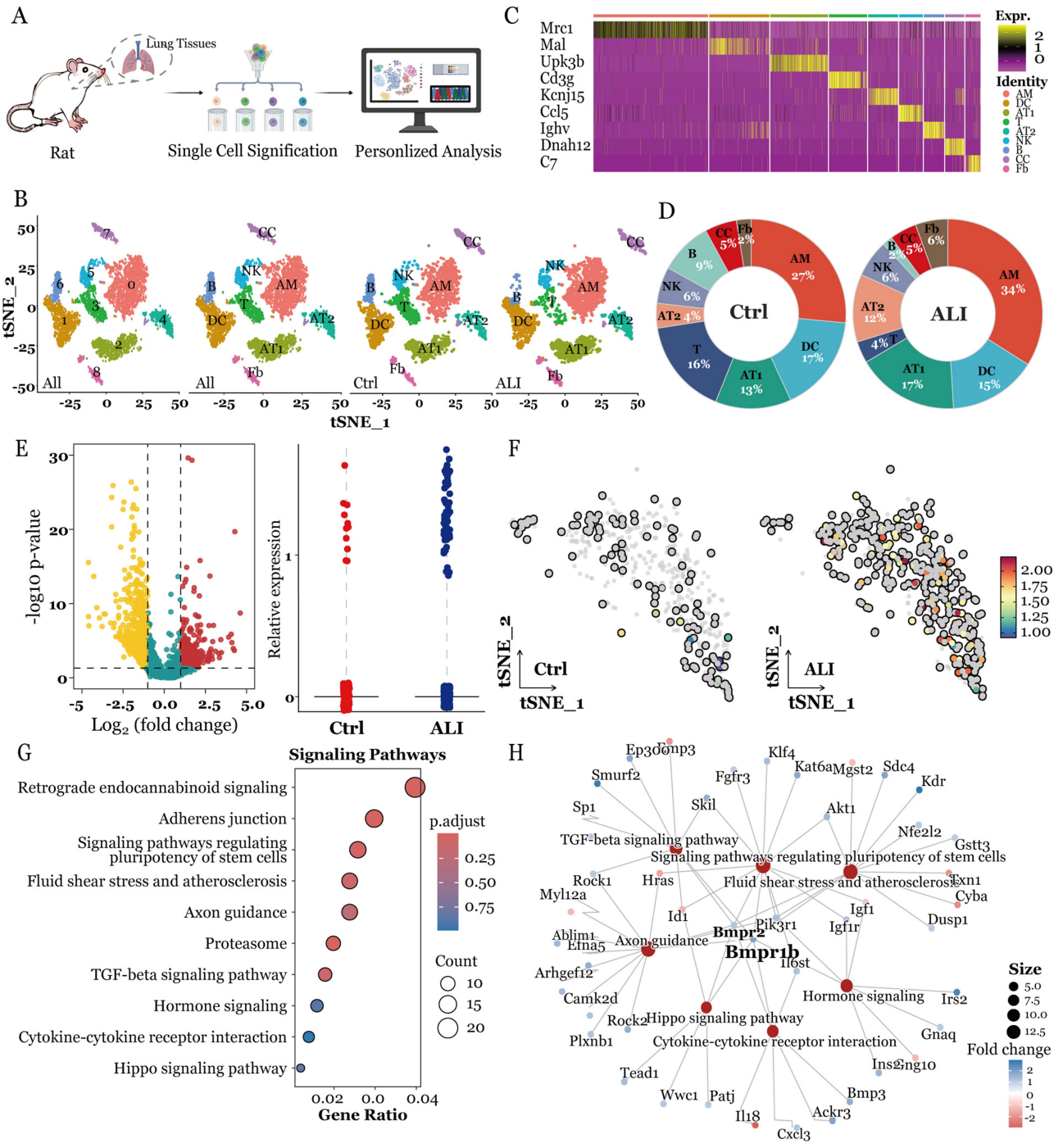

Figure 2 Single-cell RNA sequencing of acute injured lung tissue. **(A)** Schematic workflow of single-cell RNA sequencing analysis of lung tissues from ALI animals. **(B)** Scatter plots showing cell cluster enrichment and annotation analysis. **(C)** Heatmap showing expression patterns of marker genes across different cell types. **(D)** Proportional distribution of different cell populations in lung tissue across experimental groups. **(E)** Volcano plot showing ALI-induced dysregulation of genes in alveolar epithelial type II cells. **(F)** Dot plot showing the expression of BMPR1B between groups. **(G)** KEGG functional enrichment plot showing signaling pathways of interest. **(H)** Topological network visualizing BMPR1B-BMPR2 participated signaling pathways.
Abbreviation: ALI, Acute lung injury.

the docking model. Together, these results establish a detailed molecular basis for specific recognition between exosomal BMPR2 and cellular BMPR1B, supporting the potential for targeted therapeutic applications.

To systematically investigate protein-ligand interactions, quantitatively assess protein-protein interaction strength, and elucidate their functional regulatory mechanisms, we employed the Cellular Thermal Shift Assay (CETSA) to monitor

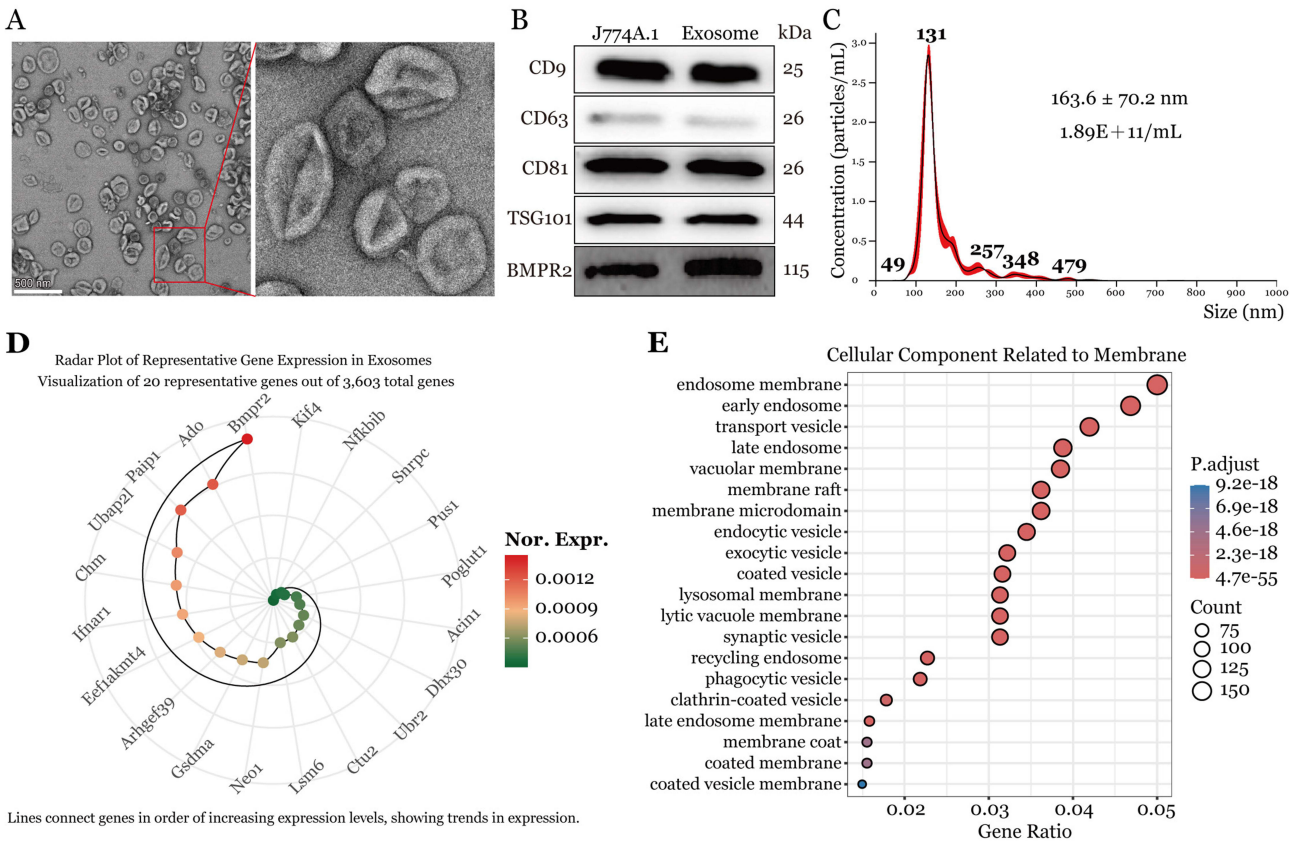

Figure 3 Smart proteomic analysis of macrophage-derived exosomes. **(A)** Transmission electron microscopy analysis of isolated exosomes showing characteristic morphology and size. Scale bar = 500 nm. **(B)** Western blot analysis of exosome marker and specificity proteins (CD9, CD63, CD81, TSG101 and BMPR2) in both J774A.1 cells and isolated exosomes. **(C)** Nanoparticle tracking analysis showing size distribution of isolated exosomes (mean size: 163.6 ± 70.2 nm; concentration: 1.89E + 11/mL). **(D)** Radar plot of representative genes packaged in exosomes. **(E)**. Functional enrichment plot showing membrane-related cellular component items.

temperature-dependent stability changes in protein complexes. Comparative analysis between the ALI and ALI+Exo groups revealed distinct thermal stability profiles. In the ALI group, BMPR2 exhibited a progressive decline in protein expression as temperature increased from 37°C to 53°C. Notably, between 45°C and 53°C, we observed a marked reduction in band signal intensity (Figure 4B), suggesting significant thermal denaturation or degradation. This temperature-sensitive behavior implies that BMPR2 possesses relatively low intrinsic thermal stability, potentially making its function susceptible to environmental temperature fluctuations or pathological conditions. In contrast, BMPR1B demonstrated greater thermal resilience, maintaining stable expression levels from 37°C to 48°C before undergoing rapid destabilization above this threshold temperature (Figure 4B). Strikingly, the ALI+Exo group showed enhanced thermostability for both receptors. Most significantly, complex formation between BMPR2 and BMPR1B induced a cooperative stabilization effect, evidenced by a synchronous rightward shift in thermal denaturation profiles (Figure 4C). This pronounced thermal stabilization suggests that heterodimerization confers structural protection, likely through interprotein interactions or stabilization of critical structural domains.

In order to further evaluate the role of the functional complex BMPR2-BMPR1B in ALI repair, at the protein level, Western blot analysis showed that the inflammatory markers IL-1β and IL-6 were downregulated in the treatment group compared to the ALI group (Figure 4D and E). These findings were also confirmed by immunohistochemistry and immunofluorescence experiments (Figure 4F-J).

Exosomal BMPR2-Mediated Signaling Promotes Repair of ALI

To evaluate the therapeutic potential of macrophage-derived exosomes for treating ALI, we first assessed their retention and stability in lung tissue through biodistribution and pharmacokinetic analyses using in vivo imaging following

https://doi.org/10.2147/IJN.S519393

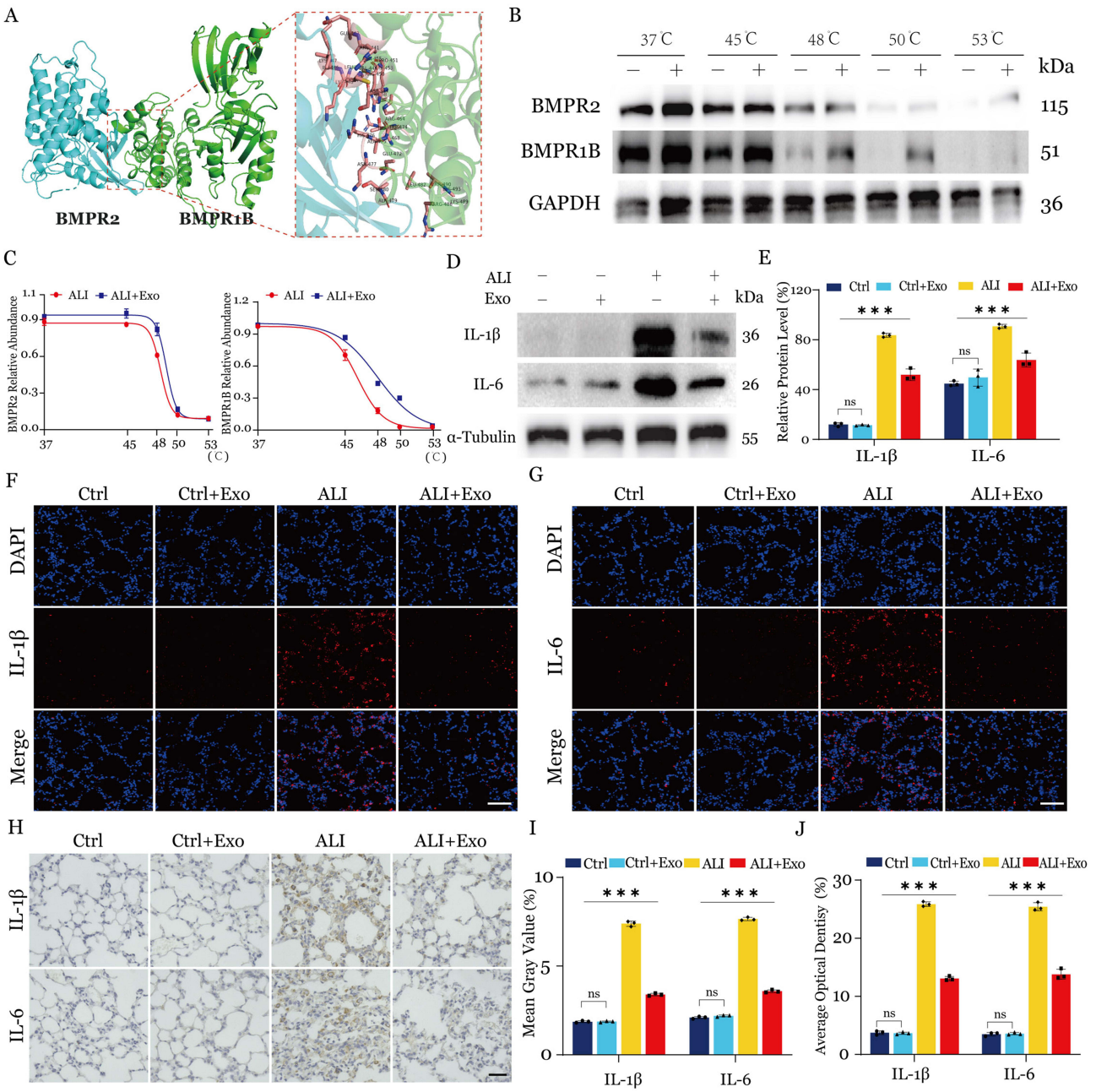

Figure 4 Molecular docking and functional validation of the BMPR2-BMPR1B complex via CETSA and inflammatory markers. **(A)** Molecular docking of exosomal BMPR2 and alveolar BMPR1B. Enlarged view: Intermolecular interactions including amino acid bonds (peptide bonds), hydrogen bonds, and hydrophobic interactions. Molecular docking scores −246.20, confidence score 0.8726, and ligand RMSD 91.98 Å (1 Å = 0.1 nm). **(B)** Western blot analysis of BMPR2 and BMPR1B protein expression under different temperature conditions (37°C, 45°C, 48°C, 50°C, and 53°C) in the presence or absence of Exosomes. **(C)** Relative abundance of BMPR2 and BMPR1B at different temperatures, assessed via CETSA. Data are represented as mean ± SD (n = 3). **(D)** Western blot showing the expression of IL-1β and IL-6 inflammatory marker proteins in lung tissue across different treatment groups. **(E)** Densitometric quantification of Western blot results for IL-1β and IL-6. **(F-G)** Immunofluorescence analysis of inflammatory markers IL-1β (**F**) and IL-6 (**G**) in lung sections (Blue: DAPI-stained nuclei; Red: target proteins). Scale bars = 200 μm. **(H)** Immunohistochemical staining of lung sections showing expression patterns of IL-1β and IL-6 across treatment groups. Nuclei are visualized in blue, with positive protein expression indicated by brown-yellow staining. Scale bar = 200 nm. **(I)** Quantification of mean gray values IL-1β and IL-6. **(J)** Average optical density analysis of IL-1β and IL-6. Data are presented as mean ± SD. Statistical significance: ***$P < 0.001$.

Abbreviation: ALI, Acute lung injury.

intratracheal administration of fluorescently-labeled exosomes at a 20 μL dose. Dynamic monitoring revealed progressive accumulation of fluorescence signal in lung tissue, initiating at 1-hour post-administration and reaching peak intensity at 4 hours, followed by gradual decline, and the pulmonary fluorescence signal was virtually undetectable by 24 hours

(Figure 5A and B). While no fluorescence was detected in the heart, liver, or kidneys before 4 hours, these organs showed non-time-dependent signal accumulation between 8–24 hours. Notably, the spleen remained devoid of fluorescence throughout the observation period, indicating preferential initial pulmonary accumulation of J774A.1 macrophage-derived exosomes followed by gradual systemic distribution, with minimal splenic retention (Figure S2). These

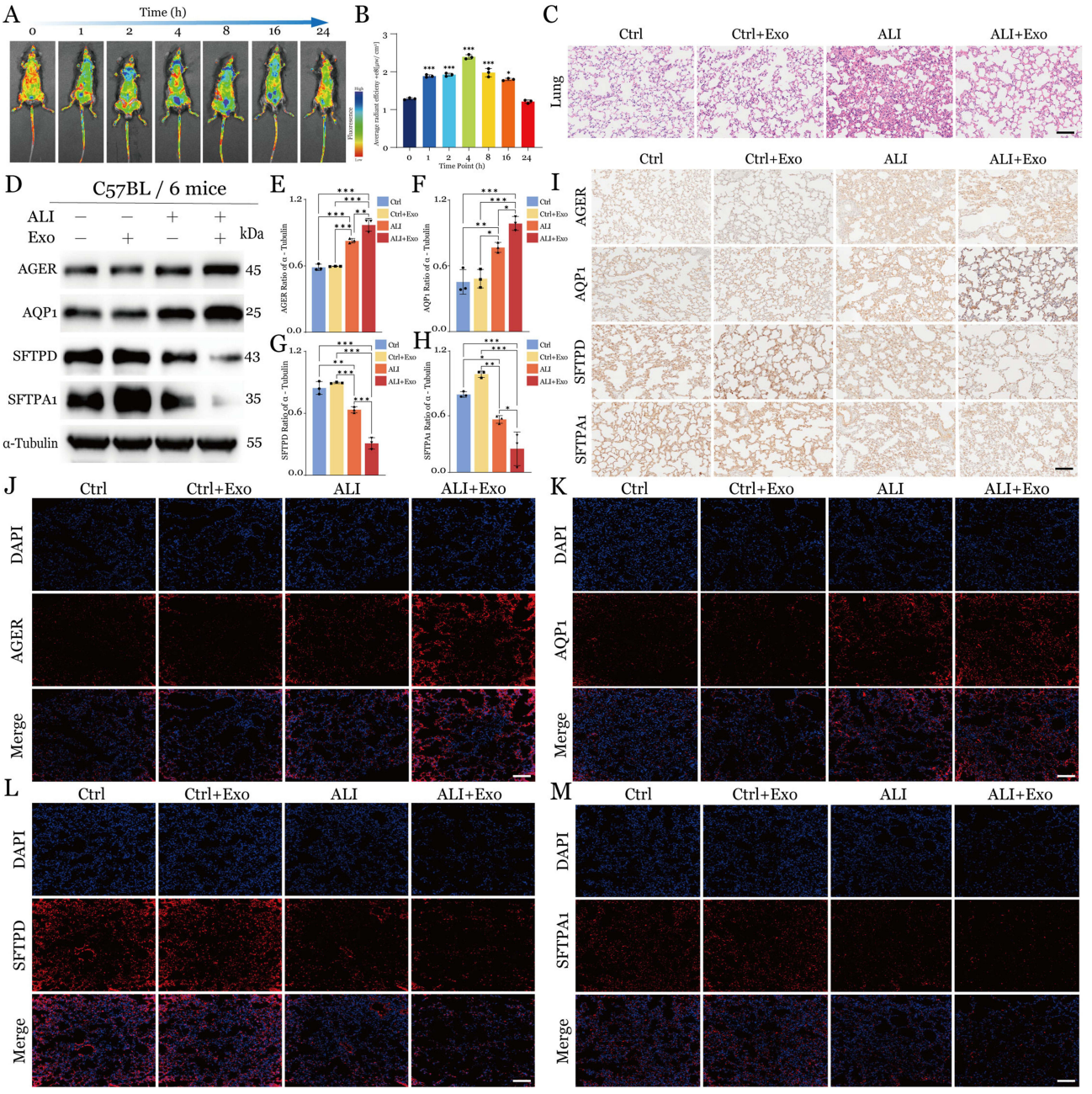

Figure 5 Therapeutic effects of macrophage-derived exosomes on lung tissue repair in ALI mice. **(A)** In vivo fluorescence imaging showing the biodistribution of DiO-labeled exosomes in mice over 24 hours. **(B)** Quantitative analysis of fluorescence intensity at different time points post-exosome administration (*$P < 0.05$, ***$P < 0.001$ compared to 0 h). **(C)** Representative H&E staining of lung sections from control, control+exosome, ALI, and ALI+exosome groups showing tissue morphology. **(D)** Western blot analysis of alveolar epithelial cell markers (AGER, AQP1, SFTPD, and SFTPA1) in lung tissue from C57BL/6 mice across different treatment groups. **(E-H)** Densitometric quantification of Western blot results for AGER (**E**), AQP1 (**F**), SFTPD (**G**), and SFTPA1 (**H**). Data are presented as mean ± SD. Statistical significance: *$P < 0.05$, **$P < 0.01$, ***$P < 0.001$. **(I)** Immunohistochemical staining of lung sections showing expression patterns of AGER, AQP1, SFTPD, and SFTPA1 across treatment groups. **(J-M)** Immunofluorescence analysis of alveolar epithelial cell markers: AGER (**J**), AQP1 (**K**), SFTPD (**L**), and SFTPA1 (**M**) in lung sections (blue: DAPI-stained nuclei; red: target proteins). Scale bars = 100 μm. Data are presented as mean ± SD. Statistical significance: ***$P < 0.001$.

Abbreviation: ALI, Acute lung injury.

https://doi.org/10.2147/IJN.S519393

biodistribution patterns demonstrate efficient pulmonary targeting and temporal retention of exosomes, providing a therapeutic window for their potential therapeutic effects.

The functional consequences of BMPR2-BMPR1B signaling were evaluated through comprehensive in vivo analyses. First, we evaluated their therapeutic efficacy in acute lung injury. Histopathological analysis through H&E staining revealed that Ctrl+Exo group maintained normal pulmonary architecture, characterized by clear alveolar spaces, thin alveolar walls with single-layer epithelium, and absence of inflammatory infiltrates, similar to Ctrl group. In contrast, the ALI group exhibited severe architectural disruption, thickened alveolar walls, and extensive inflammatory cell infiltration. Notably, the ALI+Exo group demonstrated marked improvement in pathological features, with preserved alveolar structure, reduced inflammatory infiltration, and largely restored tissue architecture, suggesting exosome-mediated enhancement of pulmonary tissue repair following ALI (Figure 5C).

At the protein level, Western blot analysis revealed progressive upregulation of AT1 markers (AGER, AQP1) and concurrent downregulation of AT2 markers (SFTPD, SFTPA1) across treatment groups compared to controls. The expression patterns showed sequential changes across Ctrl+Exo, ALI, and ALI+Exo groups, with AGER and AQP1 levels progressively increasing while SFTPD and SFTPA1 levels decreasing (Figure 5D-H). These findings were corroborated by both immunohistochemistry and immunofluorescence analyses, which confirmed the gradual upregulation of AGER and AQP1 and downregulation of SFTPD and SFTPA1 across the experimental groups (Figure 5I-M, Figure S3A-E). Data obtained in this section provide the first demonstration that ALI injury triggers transdifferentiation of AT2 to AT1, a process significantly accelerated by J774A.1 macrophage-derived exosomes, thereby enhancing recovery from ALI.

Formation of Functional BMPR2-BMPR1B Complex Activates SMAD1-Dependent Signaling and Promotes Alveolar Epithelial Cell Transdifferentiation and Repair of ALI

The molecular consequences of BMPR2-BMPR1B interaction were investigated through detailed biochemical analyses. Based on the single-cell RNA sequencing analysis, we first identified the TGF-β signaling pathway, participated by BMPR2-BMPR1B complex, as a central mediator of AT2 to AT1 transdifferentiation during ALI repair, which could be speculated that BMP proteins within the TGF-β family initiate a signaling cascade by binding to BMPRI/BMPRII receptors, leading to SMAD1/5/8 activation. Western blot analysis revealed sequential downregulation of NOGGIN and upregulation of BMPR1B and ID1 in ALI and ALI+Exo groups compared to controls (Figure 6A and B).

Since previous research has established BMPR1B as a stimulatory regulatory target for BMP-initiated TGF-β signaling.[20] BMPR1B promotes AT2 to AT1 transdifferentiation through oxidative phosphorylation-mediated stimulation of SMAD1 expression and subsequent ID1 upregulation. To further elucidate how J774A.1 macrophage-derived exosomes activate the TGF-β pathway to promote pulmonary tissue repair, we analyzed the spatial relationships between BMPR1B, SMAD1, and ID1. Triple immunofluorescence staining of lung tissue sections revealed increased fluorescence intensity of BMPR1B and ID1 in both ALI and ALI+Exo groups compared to controls, while SMAD1 showed consistently low fluorescence intensity across all groups (Figure 6C). Coexpression analysis demonstrated significant colocalization between BMPR1B and SMAD1 with a mean correlation coefficient of 0.94 ± 0.02 (Figure 6D-G). In contrast, both BMPR1B-ID1 and SMAD1-ID1 pairs showed weaker coexpression patterns, with mean correlation coefficients of 0.79 ± 0.07 and 0.72 ± 0.03, respectively (Figure S4A-H). These findings demonstrate that J774A.1 macrophage-derived exosomes accelerate the transdifferentiation of AT2 to AT1 in acute injured lung tissue through activation of the TGF-β signaling pathway.

Safety and Biodistribution Profile of BMPR2-Enriched Exosomes

To evaluate the therapeutic potential of BMPR2-enriched exosomes, we conducted comprehensive safety and biodistribution studies. Toxicological assessment revealed no apparent morphological alterations in major organs including heart, liver, spleen, lungs, kidneys, and testes across all experimental groups (Figure 7A). Quantitative analysis of body weight at day 7 demonstrated progressive weight reduction in both ALI and ALI+Exo groups compared to controls, with the ALI group showing more pronounced effects (Figure 7B).

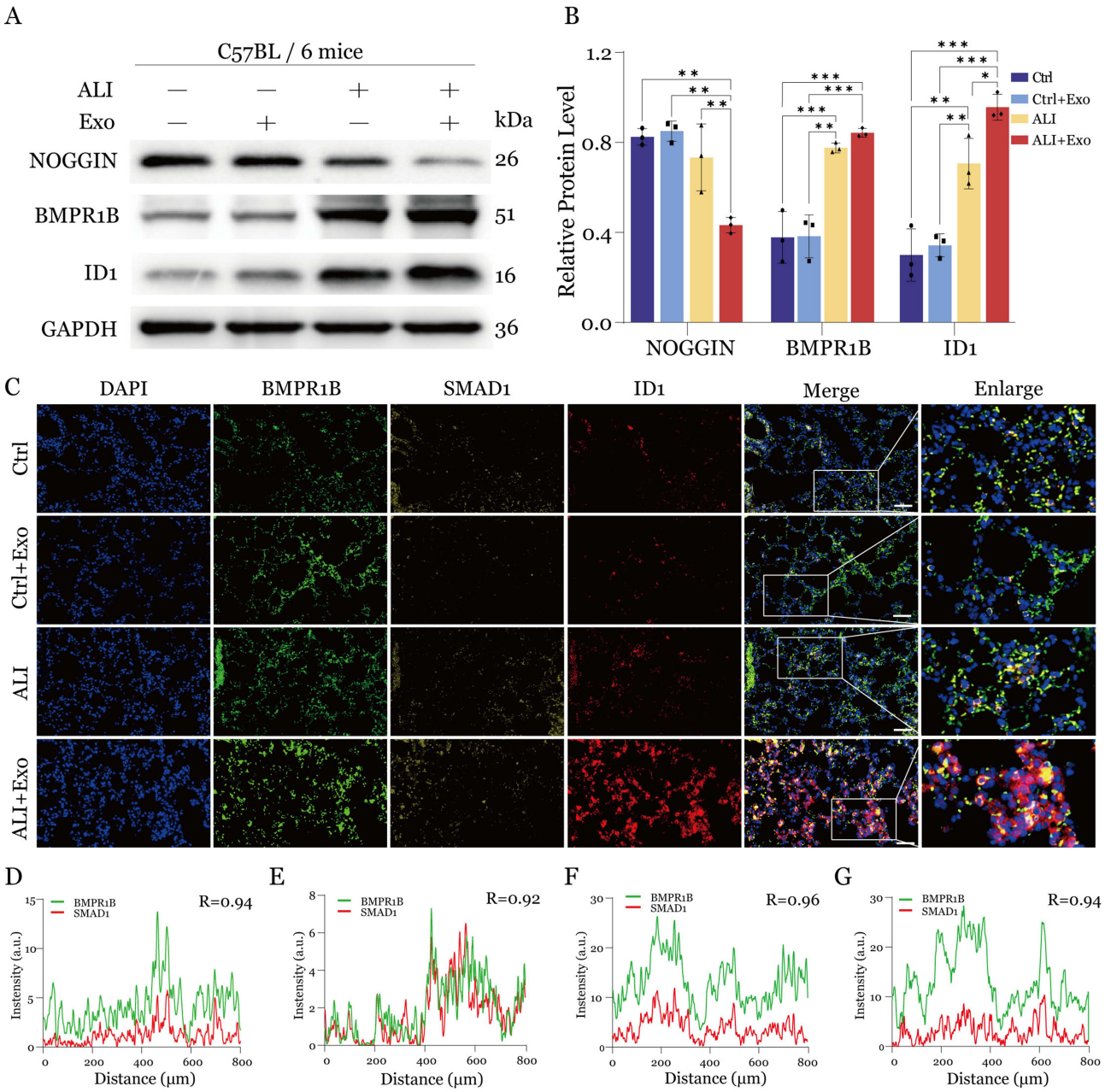

Figure 6 Role of TGF-β signaling pathway in macrophage exosome-mediated transdifferentiation of type II alveolar epithelial cells during ALI repair. **(A)** Western blot analysis of TGF-β pathway proteins in lung tissue from C57BL/6 mice across treatment groups. **(B)** Densitometric quantification of protein expression levels in mouse lung tissue. **(C)** Immunofluorescence analysis showing the expression and localization of BMPR1B, SMAD1, and ID1 across different treatment groups (blue: DAPI-stained nuclei; green: BMPR1B; yellow: SMAD1; red: ID1). Scale bar = 100 μm. **(D–G)** Correlation analysis of fluorescence intensity profiles between BMPR1B and SMAD1.(**D**), control (**E**), control+exosome (**F**), ALI (**G**), and ALI+exosome groups, with corresponding R values indicating the strength of colocalization. Data are presented as mean ± SD. Statistical significance: **P* < 0.05, ***P* < 0.01, ****P* < 0.001.
Abbreviation: ALI, Acute lung injury.

Additionally, organ coefficient analysis revealed differential effects across treatment groups. Compared to vehicle controls, the ALI group exhibited decreased pulmonary and renal coefficients alongside elevated hepatic coefficients, while other experimental groups showed no statistically significant alterations in organ coefficients (Figure 7C-G). Histopathological evaluation through H&E staining demonstrated preserved normal tissue architecture across heart, liver, spleen, and kidney specimens in all experimental groups, including controls, ALI models, and intervention groups. Microscopic examination revealed no evidence of cellular degeneration, necrosis, interstitial congestion, or edema in any

https://doi.org/10.2147/IJN.S519393

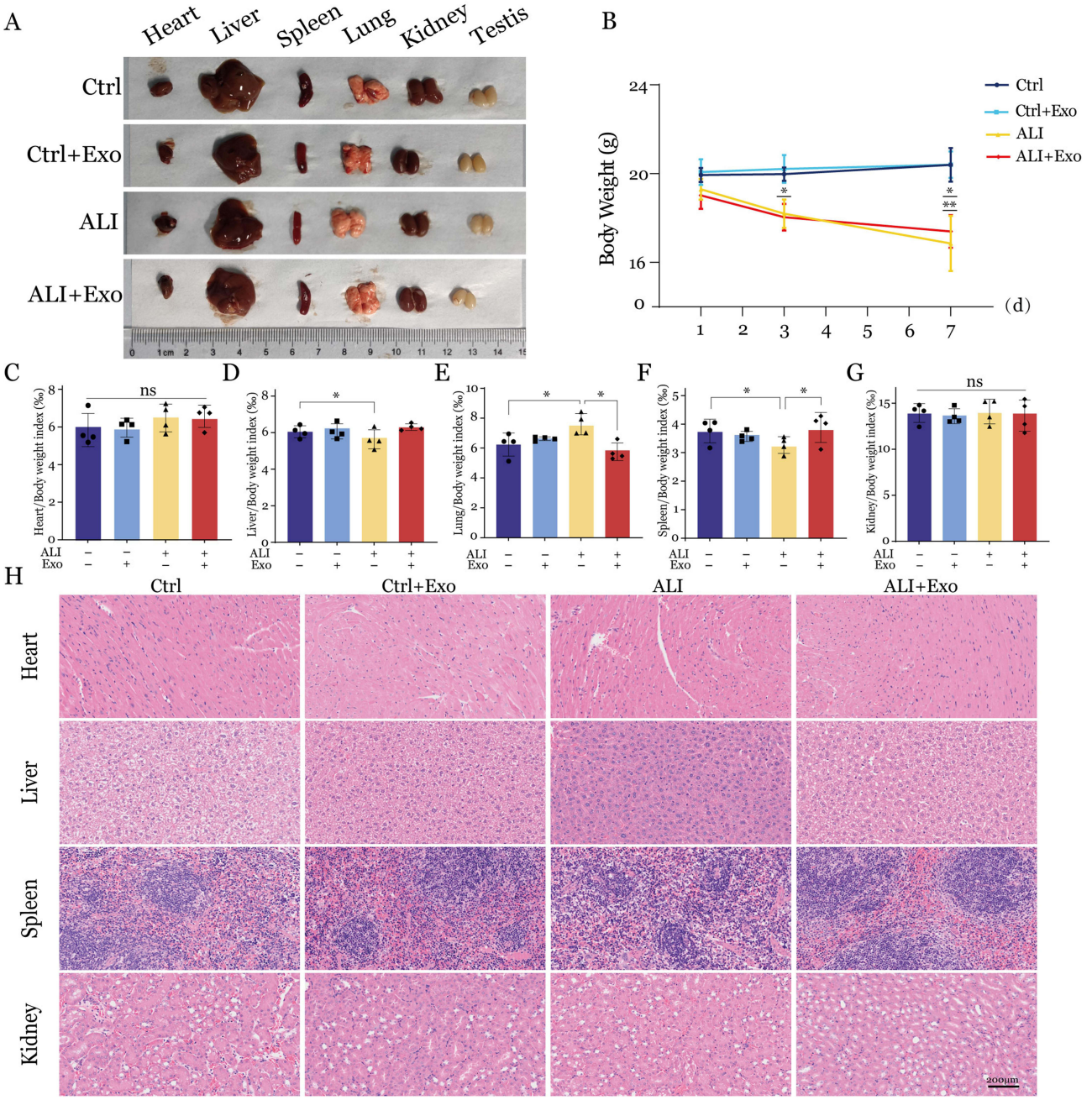

Figure 7 Safety evaluation of therapeutic macrophage-derived exosomes on systemic organs. **(A)** Representative images of major organs (heart, liver, spleen, lung, kidney, and testis) from all experimental groups. **(B)** Body weight measurements across treatment groups. **(C–G)** Organ weight indices (organ weight/body weight ratio) for heart (**C**), liver (**D**), lung (**E**), spleen (**F**), and kidney (**G**) across different treatment conditions. **(H)** Representative H&E staining of major organs (heart, liver, spleen, and kidney) showing tissue morphology across all experimental groups. Scale bar = 200 μm. Data are presented as mean ± SD. Statistical significance: $^{*}P < 0.05$, $^{**}P < 0.01$, ns: no significant.

Abbreviation: ALI, Acute lung injury.

of the examined tissues (Figure 7H). These comprehensive safety data demonstrate that while J774A.1 macrophage-derived exosomes promote AT2 to AT1 transdifferentiation through TGF-β signaling, they maintain favorable safety profiles with respect to major organ systems and physiological functions in treated mice. Importantly, the specific targeting mechanism mediated by BMPR2-BMPR1B interaction appeared to enhance therapeutic efficacy while minimizing off-target effects, supporting the potential clinical application of this approach.

Discussion

The present study provides compelling evidence for the role of exosomal BMPR2 as a key mediator of cellular repair in acute lung injury, operating through specific molecular recognition of BMPR1B on injured alveolar epithelial cells. Our findings make several significant contributions to the field of biological macromolecules and cellular repair mechanisms.

First, our proteomic characterization of macrophage-derived exosomes revealed BMPR2 as a prominently expressed surface protein, adding to the growing body of knowledge regarding exosomal membrane proteins. The presence of BMPR2 on exosomal surfaces represents a novel mechanism for intercellular communication, extending beyond its traditional role as a cellular receptor. This finding aligns with recent studies by Li et al (2023) and Li et al (2024), who demonstrated the importance of surface proteins in exosome-mediated cellular targeting, though our work is the first to specifically identify BMPR2 in this context.[21,22] Second, The molecular docking analyses and binding studies between exosomal BMPR2 and cellular BMPR1B provide crucial insights into the specificity of exosome-cell interactions. The observed docking score of −246.20 is notably stronger than previously reported interactions between soluble BMPs and their receptors, suggesting that the exosomal membrane context may enhance molecular recognition.[23] This high-affinity interaction likely contributes to the efficient cellular targeting we observed, with rapid membrane association and subsequent internalization of BMPR2-expressing exosomes. Finally Our single-cell RNA sequencing data revealed previously unrecognized complexity in the cellular response to injury, particularly regarding BMPR1B expression patterns. The observed upregulation of BMPR1B in injured alveolar epithelial cells suggests an adaptive response that enhances cellular sensitivity to BMPR2-mediated signals. This finding extends previous observations by Zhang et al (2024) and Li et al (2024), who noted altered receptor expression in various injury models, though they did not specifically examine the BMPR system.[19,24] The formation of functional BMPR2-BMPR1B complexes and subsequent activation of SMAD1-dependent signaling represents a crucial mechanistic insight. The strong colocalization between BMPR1B and phosphorylated SMAD1 (correlation coefficient 0.94 ± 0.02) demonstrates efficient signal transduction, comparable to or exceeding the efficiency reported for traditional BMP ligand-receptor interactions. This suggests that exosomal delivery of BMPR2 may provide advantages over soluble factors in activating repair pathways.

Particularly noteworthy is the ability of BMPR2-enriched exosomes to promote alveolar epithelial cell transdifferentiation. The observed phenotypic changes, characterized by coordinated regulation of cell-type specific markers, indicate a comprehensive reprogramming response that supports tissue repair. This finding builds upon work by Cuthbertson et al (2023), who demonstrated the importance of BMPR signaling in cellular plasticity, though they did not explore exosome-mediated delivery mechanisms.[25] The efficient pulmonary targeting and favorable safety profile of BMPR2-enriched exosomes support their potential therapeutic application. The peak accumulation at 4 hours post-administration provides a suitable window for biological effect, while the gradual clearance may help prevent excessive signaling. This kinetics differ from those reported by Zheng et al (2023) for non-targeted exosomes, suggesting that BMPR2-BMPR1B interactions may influence tissue distribution patterns.[26]

This study has several limitations that warrant attention. First, the experimental model was confined to blast-induced acute lung injury (ALI) in C57BL/6 mice, which does not encompass the heterogeneity of human ALI pathologies such as sepsis- or oleic acid-induced injury, potentially limiting the generalizability of the findings. Second, although the total sample size included 40 mice, the small group size (n=5 per group) may reduce statistical power to detect subtle therapeutic effects and account for inter-individual variability. Third, the therapeutic intervention focused solely on a single post-injury administration window, leaving unexplored the influence of treatment timing (eg, prophylactic or early-phase intervention) on efficacy—a critical consideration for clinical translation. Technically, while exosomes were rigorously purified and characterized, potential microvesicle contamination and batch-to-batch variability in BMPR2 content due to differences in isolation protocols or storage conditions may compromise functional consistency. Furthermore, the study primarily assessed short-term outcomes, and the long-term safety profile of exosomal therapy, including immune responses, fibrotic risks, and off-target effects, remains to be systematically evaluated. Additional mechanistic investigations are needed to clarify how the exosomal membrane context regulates BMPR2-BMPR1B binding affinity and to evaluate potential fibrotic consequences of enhanced BMP signaling. Although preclinical results are promising, translational challenges such as quality control in large-scale production and inter-patient variability must

be addressed. Future studies should systematically advance therapeutic translation by establishing diverse ALI models, expanding sample sizes, optimizing treatment protocols, and implementing comprehensive long-term safety assessments.

Future directions should focus on several key areas. Development of methods to enhance BMPR2 incorporation into exosomes could improve therapeutic efficiency. Investigation of potential synergies between BMPR2-mediated signaling and other repair pathways might identify opportunities for combination therapies. Additionally, exploration of this targeting mechanism in other tissue contexts could broaden the therapeutic applications of BMPR2-enriched exosomes. From a clinical perspective, our findings suggest several potential therapeutic strategies. The specific targeting mechanism mediated by BMPR2-BMPR1B interaction could improve delivery efficiency while reducing off-target effects. The observed safety profile supports further development toward clinical applications, though careful dose optimization studies will be needed. Additionally, the potential to modify exosome composition to enhance therapeutic efficacy while maintaining targeting specificity represents an exciting avenue for future development.

Our study also has broader implications for the field of biological macromolecules. The demonstration that exosomal presentation can enhance receptor-mediated targeting suggests similar strategies might be applicable to other therapeutic proteins. The successful maintenance of protein functionality in the exosomal membrane context provides insights for the design of other membrane-based delivery systems. Furthermore, the analytical approaches developed here could be valuable for characterizing other protein-protein interactions in complex biological systems. Several technical aspects of our work deserve consideration. The comprehensive proteomic analysis workflow we developed could be valuable for characterizing other exosome populations. The combination of molecular docking studies with functional validation provides a robust approach for investigating protein-protein interactions. Additionally, our method for tracking exosome-cell interactions could be adapted for studying other cellular targeting mechanisms.

Conclusion

In conclusion, our study establishes exosomal BMPR2 as a crucial mediator of cellular repair through specific molecular recognition of BMPR1B on target cells. These findings advance our understanding of both exosome biology and receptor-mediated cellular targeting, while providing a foundation for developing novel therapeutic strategies. Future work building upon these observations could lead to improved treatments for acute lung injury and potentially other conditions requiring targeted cellular repair.

Acknowledgment

This work was financially supported by the Taishan Scholar Program of Shandong Province (No. tsqn202211359). The funders had no role in study design, data collection, interpretation, or the decision to submit the work for publication. The study protocol received approval from the Shandong Maternal and Child Health Hospital Ethics Committee (approval reference: 2022-006). We acknowledge the ethical approval granted by the Third Affiliated Hospital of Xinxiang Medical College and express our sincere gratitude for their invaluable support and expertise in the preparation of the animal models.

Author Contributions

All authors made a significant contribution to the work reported, whether that is in the conception, study design, execution, acquisition of data, analysis and interpretation, or in all these areas; took part in drafting, revising or critically reviewing the article; gave final approval of the version to be published; have agreed on the journal to which the article has been submitted; and agree to be accountable for all aspects of the work.

Disclosure

The authors declare no competing interests in this work.

References

1. Liu C, Xiao K, Xie L. Advances in the use of exosomes for the treatment of ALI/ARDS. *Front Immunol*. 2022;13:971189. doi:10.3389/fimmu.2022.971189

2. Liu C, Xiao K, Xie L. Progress in preclinical studies of macrophage autophagy in the regulation of ALI/ARDS. *Front Immunol*. 2022;13:922702. doi:10.3389/fimmu.2022.922702
3. Mowery NT, Terzian WTH, Nelson AC. Acute lung injury. *Curr Probl Surg*. 2020;57(5):100777. doi:10.1016/j.cpsurg.2020.100777
4. Butt Y, Kurdowska A, Allen TC. Acute lung injury: a clinical and molecular review. *Arch Pathol Lab Med*. 2016;140(4):345–350. doi:10.5858/arpa.2015-0519-RA
5. Qiao X, Yin J, Zheng Z, Li L, Feng X. Endothelial cell dynamics in sepsis-induced acute lung injury and acute respiratory distress syndrome: pathogenesis and therapeutic implications. *Cell Commun Signal*. 2024;22(1):241. doi:10.1186/s12964-024-01620-y
6. Zhang L, et al. Exosomal miRNA reprogramming in pyroptotic macrophage drives silica-induced fibroblast-to-myofibroblast transition and pulmonary fibrosis. Journal of Hazardous Materials. 2025;483:136629. doi: 10.1016/j.jhazmat.2024.136629IF:12.2Q1B1
7. Chen Z, Xiong M, Tian J, Song D, Duan S, Zhang L. Encapsulation and assessment of therapeutic cargo in engineered exosomes: a systematic review. *J Nanobiotechnology*. 2024;22(1):18. doi:10.1186/s12951-023-02259-6
8. Chen Z, Yun X, Tian J, Li F, Zhang Z, Meng J, Li N, Bian H, Duan S and Zhang L. Engineering Macrophage-Derived Exosome to Deliver Pirfenidone: A Novel Approach to Combat Silicotic Pulmonary Fibrosis. Adv Healthcare Materials. 2025;14(4). doi: 10.1002/adhm.202403227
9. Tian J, Han Z, Song D, Peng Y, Xiong M, Chen Z, Duan S and Zhang L. Engineered Exosome for Drug Delivery: Recent Development and Clinical Applications. IJN. 2023;18:7923–7940. doi: 10.2147/IJN.S444582
10. Huang L, Zeng H, Jin C, et al. Sulfated galactoglucan impedes xenografted lung cancer cell growth by blocking angiogenesis via binding BMPRs. *Carbohydr Polym*. 2022;289:119412. doi:10.1016/j.carbpol.2022.119412
11. Ye Q, Taleb SJ, Zhao J, Zhao Y. Emerging role of BMPs/BMPR2 signaling pathway in treatment for pulmonary fibrosis. *Biomed Pharmacother*. 2024;178:117178. doi:10.1016/j.biopha.2024.117178
12. Fukihara J, Maiolo S, Kovac J, et al. Overexpression of bone morphogenetic protein receptor type 2 suppresses transforming growth factor β-induced profibrotic responses in lung fibroblasts. *Exp Lung Res*. 2022;48(1):35–51. doi:10.1080/01902148.2021.2024301
13. Sanchez-Duffhues G, Williams E, Goumans MJ, Heldin CH, Ten Dijke P. Bone morphogenetic protein receptors: structure, function and targeting by selective small molecule kinase inhibitors. *Bone*. 2020;138:115472. doi:10.1016/j.bone.2020.115472
14. Hopper RK, Moonen JR, Diebold I, et al. In pulmonary arterial hypertension, reduced bmpr2 promotes endothelial-to-mesenchymal transition via HMGA1 and its target slug. *Circulation*. 2016;133(18):1783–1794. doi:10.1161/circulationaha.115.020617
15. Li W, Quigley K. Bone morphogenetic protein signalling in pulmonary arterial hypertension: revisiting the BMPRII connection. *Biochem Soc Trans*. 2024;52(3):1515–1528. doi:10.1042/bst20231547
16. Yang G, Liu Y, Liu X, Yang Y. Regulation of alveolar macrophage death in pulmonary fibrosis: a review. *Apoptosis*. 2023;28(11–12):1505–1519. doi:10.1007/s10495-023-01888-4
17. Xue Y, Wang M, Han H. Interaction between alveolar macrophages and epithelial cells during Mycoplasma pneumoniae infection. *Front Cell Infect Microbiol*. 2023;13:1052020. doi:10.3389/fcimb.2023.1052020
18. Song L, Li K, Chen H, Xie L. Cell cross-talk in alveolar microenvironment: from lung injury to fibrosis. *Am J Respir Cell Mol Biol*. 2024;71(1):30–42. doi:10.1165/rcmb.2023-0426TR
19. Zhang L, Wang Y, Tian L, et al. Thrombospondin-1-mediated crosstalk between autophagy and oxidative stress orchestrates repair of blast lung injury. *Biochim Biophys Acta Mol Basis Dis*. 2024;1870(3):167026. doi:10.1016/j.bbadis.2024.167026
20. Li W, Liu Z, Wang P, et al. The transcription factor RUNX1 affects the maturation of porcine oocytes via the BMP15/TGF-β signaling pathway. *Int J Biol Macromol*. 2023;238:124026. doi:10.1016/j.ijbiomac.2023.124026
21. Li F, Yan T, Wang S, Wen X. Exosome-associated miRNA-99a-5p targeting BMPR2 promotes hepatocyte apoptosis during the process of hepatic fibrosis. *Clin Exp Med*. 2023;23(7):4021–4031. doi:10.1007/s10238-023-01122-0
22. Li Y, Xu H, Wang Y, et al. Epithelium-derived exosomes promote silica nanoparticles-induced pulmonary fibroblast activation and collagen deposition via modulating fibrotic signaling pathways and their epigenetic regulations. *J Nanobiotechnology*. 2024;22(1):331. doi:10.1186/s12951-024-02609-y
23. Qiu Y, Ying J, Yan F, et al. Novel antiosteoporotic peptides purified from protein hydrolysates of taihe black-boned silky fowl: by larval zebrafish model and molecular docking. *Food Res Int*. 2023;169:112850. doi:10.1016/j.foodres.2023.112850
24. Li L, Liu Z, Tian L, et al. Single-cell proteomics delineates murine systemic immune response to blast lung injury. *Commun Biol*. 2024;7(1):1429. doi:10.1038/s42003-024-07151-z
25. Cuthbertson I, Morrell NW, Caruso P. BMPR2 mutation and metabolic reprogramming in pulmonary arterial hypertension. *Circ Res*. 2023;132(1):109–126. doi:10.1161/circresaha.122.321554
26. Zheng W, Zhu T, Tang L, Li Z, Jiang G, Huang X. Inhalable CAR-T cell-derived exosomes as paclitaxel carriers for treating lung cancer. *J Transl Med*. 2023;21(1):383. doi:10.1186/s12967-023-04206-3